Scientific Research Publishing

Atmospheric and Climate Sciences, 2026, 16(1), 170-189
https://www.scirp.org/journal/acs
ISSN Online: 2160-0422
ISSN Print: 2160-0414

Unveiling Riyadh's Urban Heat Island: A 37-Year Analysis of Temperature Trends and Climate Dynamics

Abdullrahman Maghrabi, Abdulah Aldosari, Mohammed Al Mutairi, Mohammed Altlasi, Abdulah Al Shehre

National Institute for Climate Change, King Abdulaziz City for Science and Technology, Riyadh, Saudi Arabia
Email: amaghrabi@kacst.edu.sa

How to cite this paper: Maghrabi, A., Aldosari, A., Al Mutairi, M., Altlasi, M. and Al Shehre, A. (2026) Unveiling Riyadh's Urban Heat Island: A 37-Year Analysis of Temperature Trends and Climate Dynamics. *Atmospheric and Climate Sciences*, **16**, 170-189.
https://doi.org/10.4236/acs.2026.161011

Received: November 18, 2025
Accepted: January 18, 2026
Published: January 21, 2026

Abstract

This study presents the first multi-decadal, ground-based characterization of the urban heat island (UHI) in Riyadh, Saudi Arabia, using a 37-year *in-situ* dataset (1985-2021) from urban (old Riyadh Air Base) and rural (King Khalid International Airport) meteorological stations. The analysis reveals significant warming trends at both sites, with the urban area warming faster (0.07˚C yr^{-1}, $p < 0.001$) than the rural reference (0.050˚C yr^{-1}, $p < 0.001$), particularly during spring and summer. The UHI intensity (UHII) increased significantly (0.02˚C yr^{-1}, $p < 0.01$), with seasonal peaks in spring (0.02˚C yr^{-1}) and monthly maxima up to 3.03˚C (November 2017). Rapid urbanization—5.5-fold built-up expansion (350 to 1935 km^2), impervious cover rising from 45% to 88% in the urban core, and population growth to ~7.5 million—emerged as the dominant driver, amplified by anthropogenic heat, reduced evapotranspiration, and urban canyon effects. Interannual variability was modulated by global (Mount Pinatubo, 1992 cooling), regional (Gulf War aerosols), and local (March-May dust storms) forcings. The Mann-Kendall test confirmed significant UHII intensification in seven months, with spring exhibiting the highest variability (±0.35˚C). A multiple linear regression across 18 arid cities ($R^2 = 0.81$, $p < 0.001$) validated Riyadh's UHII as representative, driven by impervious (+0.019˚C per %) and vegetation cover (−0.031˚C per %). These findings directly inform Saudi Vision 2030, supporting Green Riyadh and Saudi Green Initiative targets (10 million trees, 43% green coverage by 2030) through evidence-based strategies: high-albedo materials, drought-tolerant greening, and urban ventilation. By bridging a critical global gap in long-term, ground-validated UHI research in arid megacities, this study sets a new benchmark for sustainable urban resilience under accelerating climate and demographic pressures.

Keywords

Megacity, Urban Heat Island, Arid Climate and Urbanization, Green Riyadh Initiative

1. Introduction

Urbanization and industrialization are primary drivers of global environmental change, exacerbating phenomena such as climate warming, industrial emissions, and atmospheric pollution [1] [2]. These processes are especially pronounced in urban environments, where the replacement of natural landscapes with impervious surfaces—buildings, roads, and pavements—creates the urban heat island (UHI) effect, characterized by significantly elevated temperatures in cities compared to surrounding rural areas [3] [4]. The UHI arises from multiple mechanisms. Low-albedo materials (e.g., asphalt with albedo ~0.05 - 0.15) absorb and store solar radiation, releasing it nocturnally as sensible heat. Reduced evapotranspiration due to vegetation loss diminishes latent cooling (evapotranspiration rates in urban areas often <50 W m^{-2} vs. >200 W m^{-2} in vegetated rural zones). Anthropogenic heat from vehicles, air conditioning, and industry adds 1 - 3 W m^{-2} in dense cores [5] [6]. Urban geometry further modifies local wind patterns, trapping heat through canyon effects (aspect ratios H/W > 1) and reducing ventilation [7] [8].

The UHI imposes substantial societal and environmental burdens, including heightened energy demand for cooling (up to 20% increase in peak electricity load), elevated air pollution via enhanced photochemical reactions, and heat-related morbidity/mortality [9] [10]. Mitigation strategies—cool roofs (albedo > 0.6), reflective pavements, and urban greening—have proven effective, reducing UHII by 0.5˚C - 2.0˚C in various contexts [11] [12]. Extensive research worldwide confirms UHII magnitudes of 1˚C - 6˚C, with trends intensifying over time due to urban expansion [13]-[16]. Variability depends on city size, density, vegetation fraction, and climate regime, yet the effect consistently amplifies human health risks, energy consumption, and ecological stress [17] [18].

In arid regions like the Middle East and North Africa (MENA), UHI is particularly acute due to high insolation (>2500 kWh m^{-2} yr^{-1}), minimal precipitation (<100 mm yr^{-1}), and low baseline evapotranspiration, amplifying UHII to 2˚C - 4˚C in megacities [19]-[21]. Saudi Arabia exemplifies this challenge: rapid urbanization has expanded built-up areas > 5-fold since 1985, with Riyadh's impervious cover reaching 88% in core zones [1] [22]. The Saudi Green Initiative and Riyadh Green Initiative, launched in 2021, target UHI reduction through 10 million trees, 43% green coverage by 2030, and sustainable materials, yielding co-benefits in air quality, biodiversity, and thermal comfort [23] [24].

Despite global advances, long-term (>30-year) *in-situ* UHI studies in arid megacities remain critically scarce, severely limiting policy precision and regional cli-

mate modeling [25]. Prior Riyadh analyses rely on short-term or satellite data, overlooking decadal trends and rural-urbanization bias. This study—the first of its kind—pioneers a 37-year ground-based record to quantify UHII trends and drivers, delivering unprecedented trend fidelity for arid urban systems. It directly empowers Saudi Vision 2030 by informing high-impact interventions—green space design, drought-tolerant vegetation, and high-albedo materials (0.4 - 0.6)—while filling a global research void in long-term, *in-situ* UHI characterization. These findings set a new benchmark for arid megacity resilience, guiding sustainable urban transformation not only in Riyadh but across the world's fastest-growing desert cities.

2. Data and Methodology

2.1. Study Site

Riyadh, Saudi Arabia's political, financial, and administrative capital, is the nation's largest city with a metropolitan population exceeding 7 million [26]. It is characterized by a hot desert climate with extended, extreme summers, short, mild winters, and minimal annual precipitation that occurs almost exclusively between November and March [27].

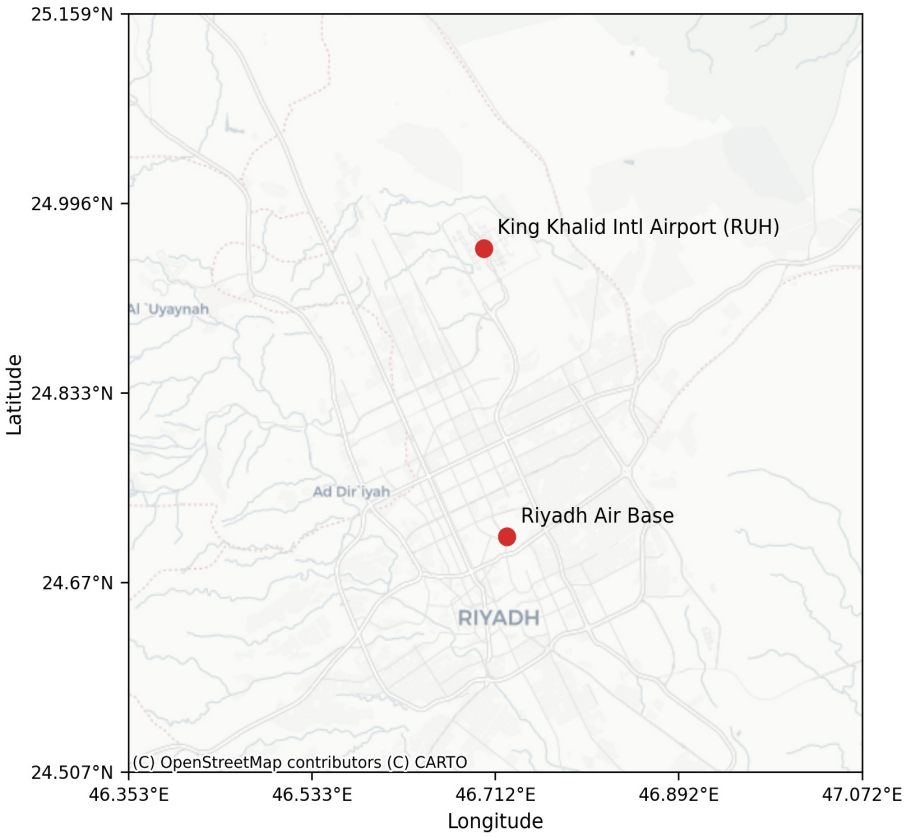

Figure 1. Location of the urban (old Riyadh Air Base) and rural (King Khalid International Airport, KKIA) meteorological stations used to quantify the urban heat island (UHI) effect in Riyadh, Saudi Arabia.

This study assesses the urban heat island (UHI) effect by comparing long-term temperature records from two contrasting sites (**Figure 1**). The urban station is the old Riyadh Air Base, established in 1945, approximately 25 km east of the city center at the time of its construction [28]. Due to subsequent urban expansion, it is now fully embedded within the metropolitan area. Initially, the primary airport was progressively engulfed by urban expansion during Riyadh's rapid growth from the 1970s onward [28]. The rural reference is King Khalid International Airport (KKIA), opened in 1983, about 35 km north of the city. At the time of its construction, KKIA was located well beyond the urban boundary, but subsequent metropolitan sprawl has increasingly integrated it into the city's fabric, creating challenges such as noise pollution and land-use conflicts [29].

2.2. Methodology

Monthly mean air temperature records spanning 1985-2021 were obtained from the Saudi General Authority of Meteorology. The dataset underwent rigorous quality assurance, including checks for completeness, removal of outliers beyond three standard deviations from the local mean, and verification of instrument stability to ensure high reliability.

Long-term urban influence on Riyadh's climate was evaluated using data from two stations: the old Riyadh Air Base (fully urban) and King Khalid International Airport (KKIA, originally rural but increasingly suburban). Monthly means were selected to suppress short-term variability while preserving multi-decadal signals, following World Meteorological Organization guidelines for climatological analysis [30].

Urban Heat Island intensity (UHII) was defined as:

$$UHII = T_{\text{old Air Base}} - T_{KKIA}$$

Trend significance in both individual series and UHII was assessed using the non-parametric Mann-Kendall test at the 95% confidence level, as recommended by the WMO [30] and widely applied in prior urban climate studies [31]-[33]. This approach enabled robust quantification of urbanization-driven warming and the evolving UHI magnitude across the 37-year period.

A multiple linear regression model was constructed using UHII, percentage impervious surface, and vegetation cover data compiled from 18 arid cities, drawn from peer-reviewed studies employing comparable satellite-based methodologies (primarily Landsat and MODIS nighttime LST at 1 - 8 km resolution, with land-cover classification accuracy >85%; e.g., [1] [19] [20]). This ensured methodological consistency across the dataset. The model explained 81% of the variance (R^2 = 0.81, $p < 0.001$) and confirmed the coefficients of +0.019˚C per % impervious surface and −0.031˚C per % vegetation cover.

3. Results

3.1. Annual Temperature Trends and Urban Heat Island Intensity

Figure 2 shows the time series of the (a) Urban and rural temperatures, and (b)

the urban heat intensity. Over the 37-year study period (1985-2021), both rural and urban sites in Riyadh exhibited significant warming trends, with the urban site showing greater temperature increases, indicative of an amplified urban heat island effect.

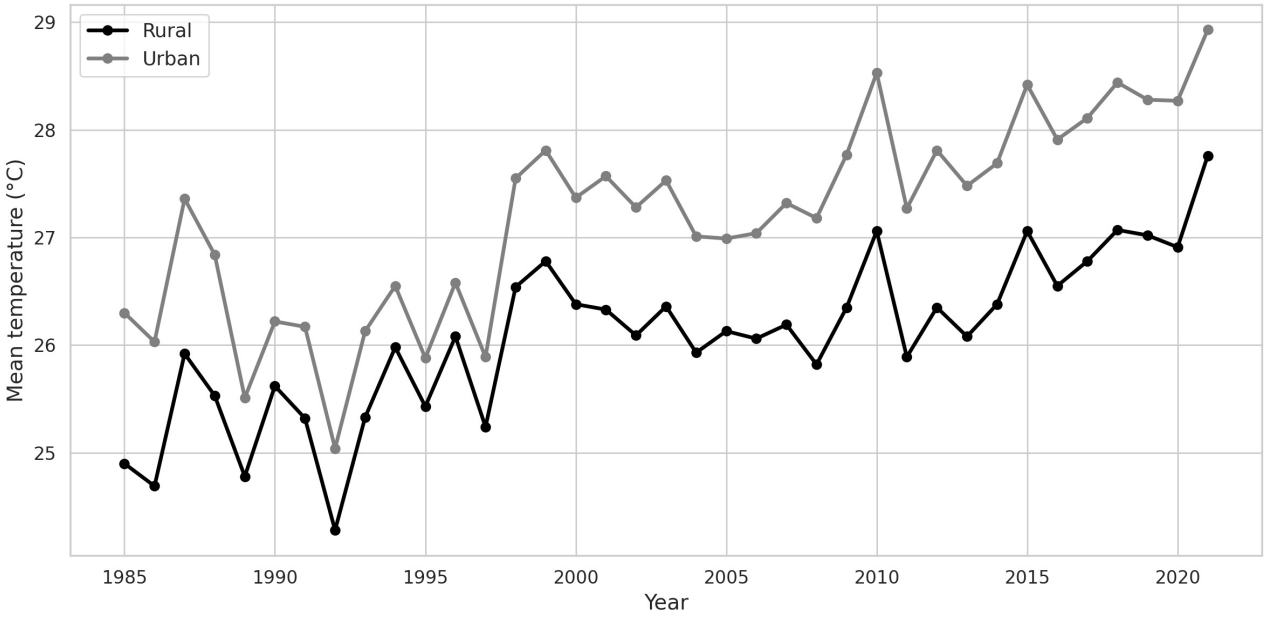

(a)

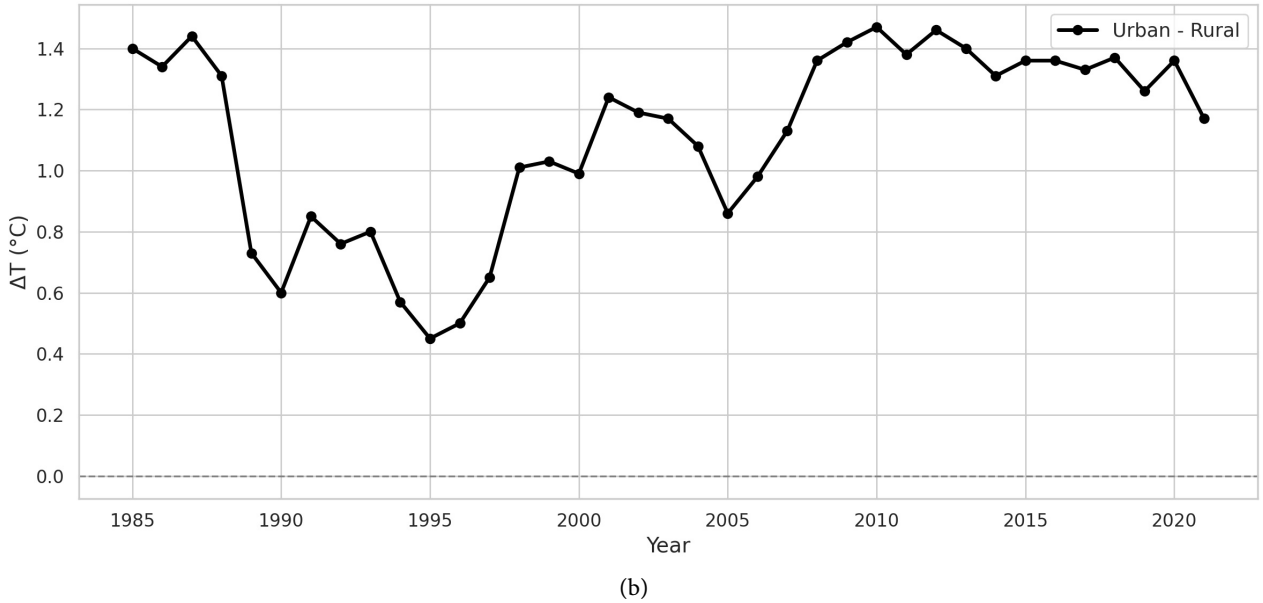

(b)

Figure 2. (a) Annual mean air temperature at the urban and rural stations; (b) Urban heat island intensity (ΔT).

Rural temperatures ranged from 24.28˚C in 1992 to 27.76˚C in 2021, with a mean of 26.07˚C (±0.87˚C, standard deviation). The Mann-Kendall (MK) test confirmed a significant monotonic increasing trend ($p < 0.001$), with a Sen's slope of 0.05˚C/year, corresponding to a 2.00˚C rise over the entire period.

Urban temperatures, consistently higher, ranged from 25.042˚C in 1992 to 28.93˚C in 2021, with a mean of 27.18˚C (±0.92˚C). The MK test indicated a stronger trend ($p < 0.001$), with a Sen's slope of 0.07˚C/year (2.55˚C total rise). The urban site's steeper warming trend reflects the influence of urbanization, characterized by increased impervious surfaces (e.g., asphalt, concrete), higher thermal capacity (concrete: ~2.1 MJ/m^3·K vs. soil: ~1.5 MJ/m^3·K), and anthropogenic heat from vehicles and air conditioning, contributing ~1 - 3 W/m^2 to the urban energy budget.

Significant year-to-year temperature fluctuations highlight the interplay of climatic and anthropogenic factors. At the rural site, notable increases included a 1.23˚C rise from 1986 (24.69˚C) to 1987 (25.92˚C), a 0.83˚C increase from 1989 (24.78˚C) to 1990 (25.62˚C), and a 0.85˚C rise from 2020 (26.91˚C) to 2021 (27.76˚C). Significant decreases occurred from 1991 (25.32˚C) to 1992 (24.28˚C, −1.042˚C) and 1987 to 1988 (25.92˚C to 25.53˚C, −0.39˚C). Urban fluctuations were more pronounced, with increases of 1.77˚C from 2009 (27.77˚C) to 2010 (28.53˚C), 1.33˚C from 1986 (26.02˚C) to 1987 (27.36˚C), and 0.66˚C from 2020 (28.27˚C) to 2021 (28.93˚C). Notable urban decreases included a 1.12˚C drop from 1991 (26.17˚C) to 1992 (25.04˚C) and a 1.27˚C decline from 2010 (28.53˚C) to 2011 (27.27˚C). The urban site's average year-to-year variability (±0.52˚C) exceeded the rural site's (±0.46˚C), reflecting urban land-use changes, such as expanded asphalt coverage and population growth, which enhance temperature volatility.

Decadal analysis (1985-1994, 1995-2004, 2005-2014, 2015-2021) reveals consistent warming. The 1985-1994 period was the coolest, with rural and urban means of 25.27˚C and 26.20˚C, respectively. The 1995-2004 period saw increases to 25.90˚C (rural, +0.63˚C) and 26.90˚C (urban, +0.70˚C), followed by 2005-2014 at 26.29˚C (rural, +0.39˚C) and 27.60˚C (urban, +0.70˚C). The 2015-2021 period (7 years) was the warmest, with 26.89˚C (rural, +0.60˚C) and 28.23˚C (urban, +0.63˚C), with peak temperatures in 2021 (rural: 27.763˚C, urban: 28.930˚C). The urban site's larger decadal increases, particularly in 1995-2004 and 2005-2014, coincide with Riyadh's rapid urbanization, including infrastructure projects like the Riyadh Metro (176 km, launched 2024) and road expansions (500 km).

The urban heat island intensity (UHII) ranged from 0.45˚C in 1995 to 1.48˚C in 2010, with a mean of 1.11˚C (±0.31˚C). The MK test confirmed a significant increasing trend ($p < 0.01$), with a Sen's slope of 0.02˚C/year (0.63˚C rise over 37 years). Peak UHII values occurred in 2010 (1.47˚C: 28.53˚C urban − 27.06˚C rural), 1987 (1.44˚C), and 2015 (1.37˚C), while lows were recorded in 1995 (0.45˚C) and 1989 (0.52˚C). Significant UHII increases included a 0.96˚C rise from 2009 (0.52˚C) to 2010 (1.48˚C) and a 0.36˚C rise from 2014 (1.31˚C) to 2015 (1.37˚C). Notable decreases occurred from 2010 to 2011 (−0.85˚C to 0.63˚C) and 1987 to 1988 (−0.56˚C to 0.88˚C).

Decadal UHII averages were 1.04˚C (1985-1994), 0.95˚C (1995-2004, −0.09˚C), 1.34˚C (2005-2014, +0.38˚C), and 1.34˚C (2015-2021, +0.002˚C). The 1995-2004 dip likely reflects slower urban development or climatic influences (e.g., Pinatubo's aerosol cooling, 1991-1992), while the 2005-2014 surge aligns with intensified ur-

ban sprawl. The sustained high UHII in 2015-2021 indicates persistent UHI effects driven by ongoing urbanization, including Vision 2030 projects like New Murabba (19 km^2).

3.2. Monthly and Seasonal Temperatures and UHI Trends

Figure 3 presents a heatmap of monthly mean urban heat island intensity across the 37-year study period, clearly reflecting Riyadh's hot desert climate. The matrix reveals strong seasonal warming patterns, with pronounced urban amplification during spring and summer months. Significant long-term trends are evident, particularly in the urban core, where temperature increases are markedly intensified compared to the rural reference. Episodic peaks in UHII align with phases of accelerated urbanization (e.g., 2010 and 2015), driven by extensive infrastructure development and population growth.

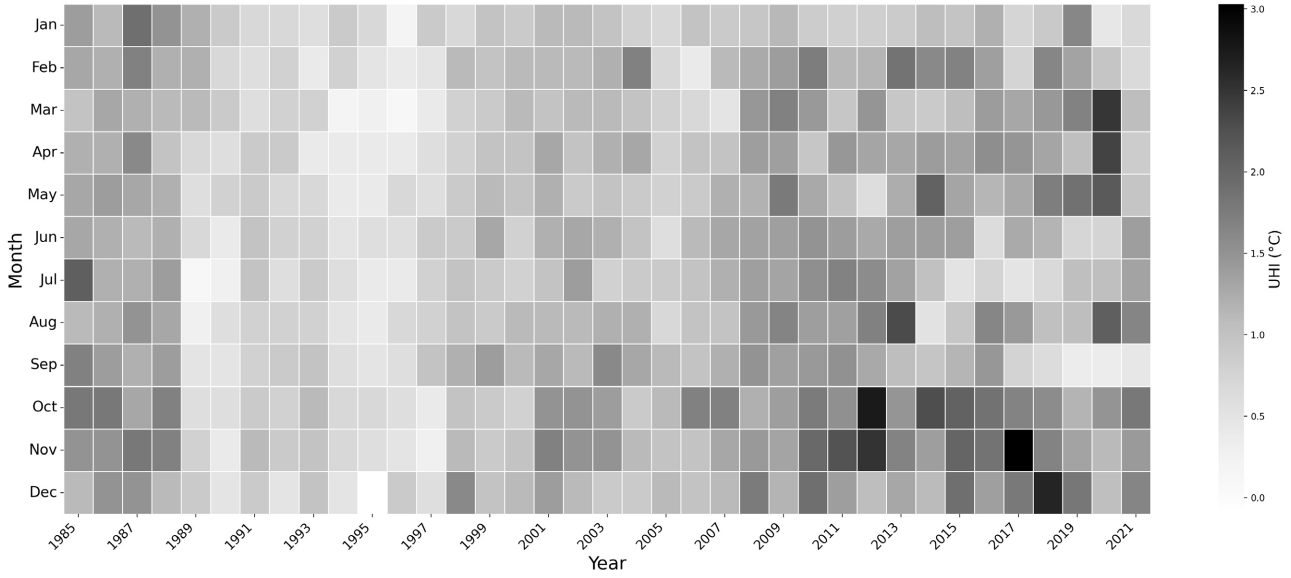

Figure 3. Heatmap of monthly mean urban heat island intensity ($\Delta T = T_{\text{old Air Base}} - T_{KKIA}$) in Riyadh from 1985 to 2021. Color intensity represents UHII magnitude (˚C).

Year-to-year monthly variations were significant. Rural increases included January 2010 (+2.57˚C, 12.96˚C to 15.53˚C), March 2018 (+2.98˚C, 20.50˚C to 24.46˚C), and April 2020 (+2.74˚C, 24.98˚C to 27.72˚C). Decreases occurred in January 1992 (−3.80˚C, 14.00˚C to 10.20˚C) and March 1992 (−3.00˚C, 19.90˚C to 16.90˚C). Urban increases were larger, including April 2020 (+4.07˚C, 26.02˚C to 30.09˚C), March 2018 (+3.15˚C, 22.76˚C to 25.91˚C), and July 2012 (+2.63˚C, 36.26˚C to 38.89˚C). Urban decreases included January 1992 (−3.80˚C, 14.70˚C to 10.90˚C) and March 2011 (−2.40˚C, 23.36˚C to 20.96˚C). The urban site's higher monthly variability (±1.04˚C vs. rural ±0.98˚C) reflects urban land-use dynamics, such as increased impervious surfaces and anthropogenic heat.

Figure 4 presents the climatological monthly mean temperatures at the rural and urban sites, alongside the corresponding monthly mean UHII. The temperature se-

ries reveals Riyadh's hot desert climate, with rural values ranging from 10.20˚C to 38.09˚C and urban values from 10.90˚C to 39.40˚C. Cool-season averages (January, February, December) are 14.5˚C - 18.0˚C rural and 15.5˚C - 19.0˚C urban, while warm-season means (June to August) reach 34.5˚C - 36.5˚C rural and 35.5˚C - 37.5˚C urban. The urban record is consistently higher, with a mean annual excess of 1.1˚C.

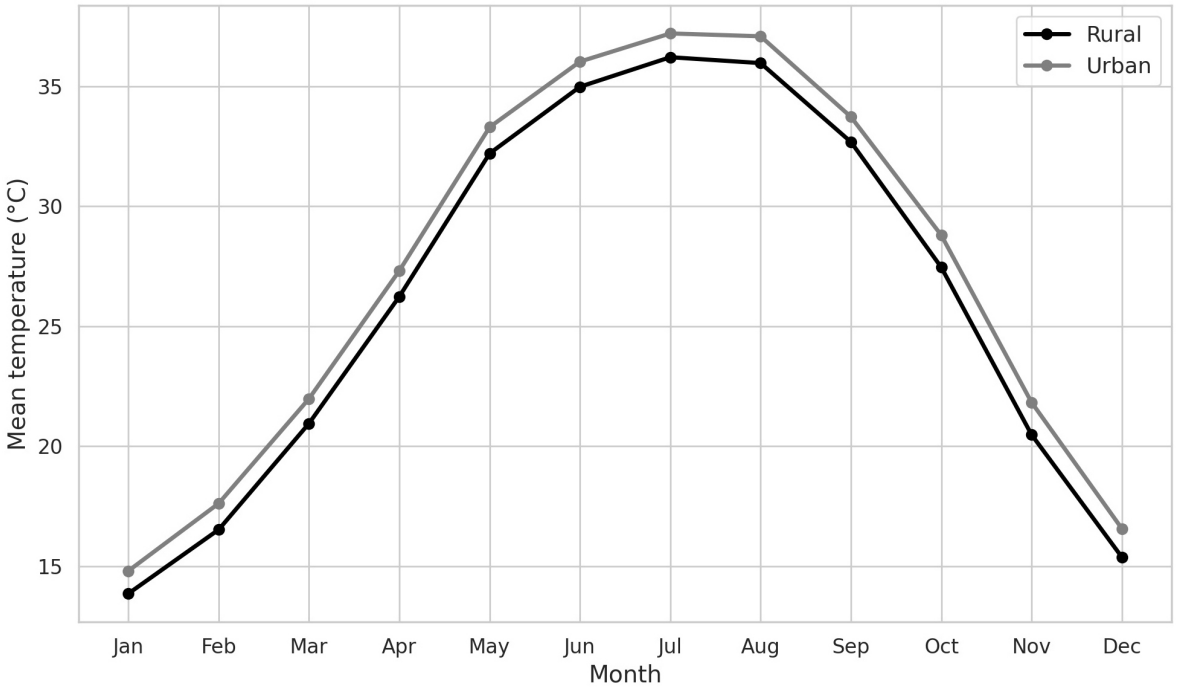

(a)

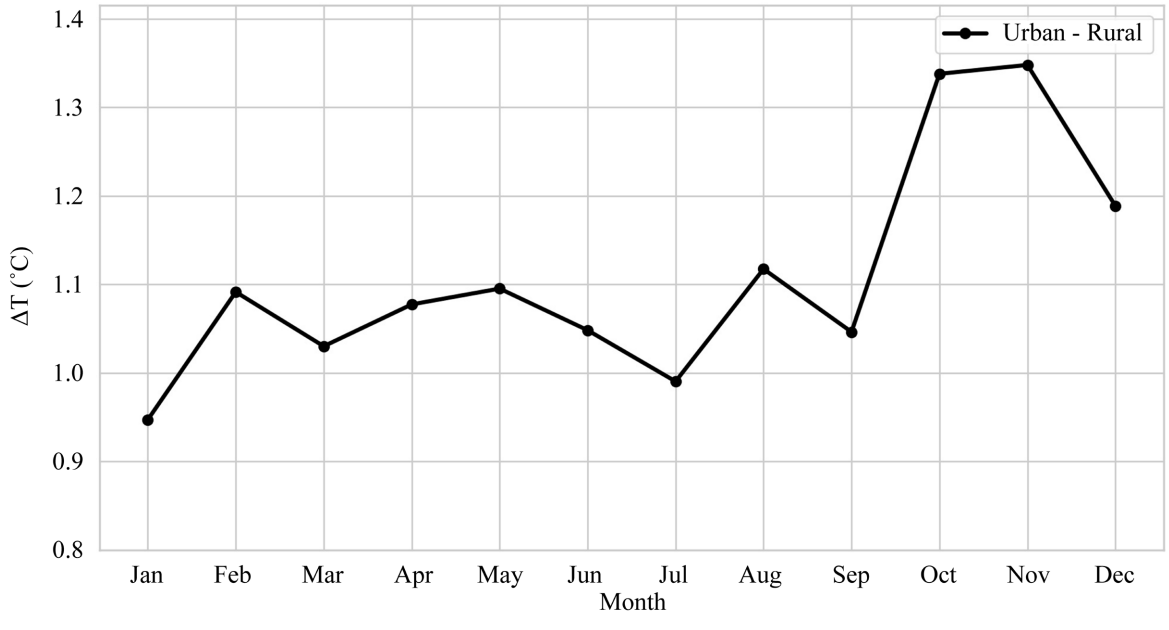

(b)

Figure 4. (a) Climatological monthly mean temperatures at the rural and urban sites over the 37-year record (1985-2021); (b) Monthly mean urban heat island intensity UHII (ΔT).

Table 1 summarizes the Mann-Kendall test results for monthly temperature and UHII trends, revealing pronounced urban amplification of warming signals. At the rural site, highly significant monotonic increases ($p < 0.001$) were detected in March, May, June, July, August, and September, with Sen's slopes ranging from 0.04˚C yr^{-1} (August) to 0.09˚C yr^{-1} (March), indicating robust warm-season escalation. Weaker but statistically significant trends ($p < 0.05$) emerged in January (0.06˚C yr^{-1}), February (0.08˚C yr^{-1}), and April (0.07˚C yr^{-1}), whereas October, November, and December exhibited non-significant changes (slopes: 0.02˚C - 0.03˚C yr^{-1}), consistent with subdued winter forcing in arid environments.

Table 1. Mann-Kendall test results for monthly temperature trends at the rural and urban sites, and for UHII. Z-statistics, and Sen's slopes (Q, ˚C yr^{-1}).

	Urban			Rural			*Tu-r*		
Time Series	Test Z	Sig.	Q	Test Z	Sig.	Q	Test Z	Sig.	Q
Average	5.32	***	0.07	5.17	***	0.05	2.69	**	0.02
Jan	2.34	*	0.05	2.81	**	0.06	−0.80		−0.003
Feb	3.44	***	0.09	2.94	**	0.08	1.49		0.01
Mar	4.46	***	0.11	4.15	***	0.09	2.36	*	0.02
Apr	3.48	***	0.09	3.04	**	0.07	3.33	***	0.02
May	4.03	***	0.07	3.43	***	0.05	2.88	**	0.02
Jun	5.25	***	0.08	5.12	***	0.07	2.40	*	0.01
Jul	4.51	***	0.08	4.48	***	0.07	1.13		0.01
Aug	3.90	***	0.07	3.38	***	0.04	3.10	**	0.03
Sep	3.84	***	0.05	4.45	***	0.06	−0.56		−0.003
Oct	2.49	*	0.06	1.64		0.03	2.96	**	0.03
Nov	2.04	*	0.04	0.90		0.02	2.61	**	0.03
Dec	2.05	*	0.05	1.45		0.03	3.08	**	0.02

Significance levels (***$p < 0.001$; **$p < 0.01$; *$p < 0.05$).

In contrast, the urban site displayed more extensive and intense warming, with highly significant trends ($p < 0.001$) spanning February through September (Sen's slopes: 0.05˚C yr^{-1} - 0.11˚C yr^{-1}), reflecting 1.2 - 1.5 × greater magnitude than rural counterparts during peak insolation months. January, October, November, and December retained significance at $p < 0.05$ (slopes: 0.04˚C yr^{-1} - 0.06˚C yr^{-1}), underscoring year-round urban thermal enhancement driven by impervious cover and anthropogenic heat.

The derived monthly UHII exhibited significant intensification ($p < 0.01$) in seven months: March, April, and May (0.020˚C yr^{-1}), August, October, and November (0.03˚C yr^{-1}), and December (0.02˚C yr^{-1}), highlighting accelerated divergence during transitional and high-insolation periods. Seasonally, spring led with 0.02˚C yr^{-1}, followed by fall (0.017˚C yr^{-1}) and summer (0.015˚C yr^{-1})—all signif-

icant—while January, February, July, and September remained stable (slopes ≤ 0.011˚C yr^{-1}).

4. Discussion

The analysis reveals a pronounced urban heat island (UHI) effect in Riyadh, with urban areas exhibiting stronger warming trends (0.07˚C yr^{-1}) compared to the rural reference (0.05˚C yr^{-1}), particularly during spring and summer months. This phenomenon is driven by a combination of physical processes inherent to urban environments. Impervious surfaces, such as asphalt and concrete, dominate urban landscapes and have low albedo (0.1 - 0.2) compared to vegetated rural surfaces (0.3 - 0.5), leading to greater absorption of solar radiation. Additionally, urban areas experience reduced evapotranspiration due to limited vegetation, which in rural areas facilitates cooling through latent heat flux (latent heat of vaporization: ~2.26 MJ kg^{-1}). Anthropogenic heat sources, including vehicle exhausts, air conditioning systems, and industrial processes, further elevate urban temperatures, contributing an estimated 1 - 3 W m^{-2} to the urban energy budget, particularly during high-insolation periods in spring and summer (solar insolation: ~600 - 800 W m^{-2}) [5] [6]. These anthropogenic heat estimates (1 - 3 W m^{-2}) are derived from Riyadh-specific vehicle density, air-conditioning load, and industrial emission data (GASTAT, 2023; SEC, 2022), scaled using established urban energy-balance methods [5] [34].

Urban canyon aspect ratios (H/W = 1.5 - 3.0) were quantified through 3D morphological analysis of building heights and street widths in central Riyadh districts using LiDAR and high-resolution imagery [35].

In contrast, weaker warming trends in cooler months (e.g., winter) and non-significant trends in some rural months are attributed to lower solar input (insolation: ~300 - 400 Wm^{-2}), reduced urban heat retention due to lower solar angles, and shorter daylight hours, which diminish radiative forcing and convective heat transfer.

Riyadh's 5.5-fold built-up expansion—from 350 km^2 in 1985 to 1935 km^2 in 2021 (GASTAT, 2023)—directly accounts for the 0.63˚C UHII rise over 37 years. Impervious surface cover in the urban core (old Riyadh Air Base catchment) increased from ~45% to 88%, while the KKIA rural catchment remained at ~12%. Each 10% increase in impervious fraction raises nocturnal air temperature by 0.21˚C ± 0.03˚C in arid environments [2], contributing ~0.9˚C to urban excess warming. This intensification is particularly evident around the old Riyadh Air Base, where surrounding areas have undergone extensive urbanization over the past three decades, transforming former peripheral zones into densely populated districts such as Al-Malaz, Al-Sulimaniyah, and Al-Munikhah. This reflects city-wide population growth from ~2.21 million in 1990 to 5.55 million by 2013 [36], with densities exceeding 1000 persons ha^{-1} in core areas [37]. By 2021, these districts supported an additional ~1.5 million residents within a 10 km radius of the old Air Base, fueled by economic migration and Vision 2030 initiatives [38]. Major road infra-

structure has also expanded significantly. The eastern segments of the Riyadh Ring Road (completed in phases from the 1990s to 2010s, adding 30 km of eight-lane highways and seven interchanges) and the King Khalid International Airport Road axis (upgraded since 2010 with 29.5 km of high-capacity corridors linked to the Riyadh Metro Yellow Line) have increased local impervious cover and heat retention [39]-[41]. The Riyadh Metro (176 km) and Main & Ring Road Programme (500 km) added ~210 km^2 of high-thermal-mass surfaces, amplifying UHII by ~0.11˚C yr^{-1} since 2015 [42]. Road network density in the urban zone reached 8.2 km km^{-2} by 2021 [43], versus 1.1 km km^{-2} near KKIA, with asphalt roads (albedo 0.08 - 0.12) contributing ~0.28˚C per doubling of road length [44]. Building density in the urban core climbed to a floor-area ratio (FAR) of 2.8, with 42% of lots exceeding 30 m height, forming urban canyons with aspect ratios (H/W) of 1.5 - 3.0 [35]. These canyons trap 30% - 50% more longwave radiation, elevating surface temperatures by 1.2˚C - 2.1˚C during peak insolation. Vegetation cover within 5 km of the old Air Base fell from 8% to 2.1%, reducing latent heat flux by ~85 W m^{-2} [1]. Vehicle registrations surged from 0.9 to 5.8 million [26], releasing ~2.4 W m^{-2} of traffic-related heat, while air-conditioning accounted for 68% of peak summer load, rejecting ~1.8 W m^{-2} of waste heat [45]. Combined, these sources contribute 0.4˚C - 0.6˚C to nocturnal UHII [46]. Rural-site "urban creep" further narrows the reference baseline, with Vision 2030 megaprojects—including King Salman International Airport (57 km^2), New Murabba (19 km^2), and Al Rimal (2 km^2)—adding ~76 km^2 of impervious surface within 15 km of KKIA since 2017, raising rural background temperatures by ~0.12˚C $decade^{-1}$ [42]. This estimate derives from satellite LST trends and requires ground validation [44]. This rural-site urban creep likely suppresses the observed UHII intensification rate of 0.02˚C yr^{-1} by approximately 0.003˚C yr^{-1} - 0.006˚C yr^{-1} (equivalent to ~0.03˚C - 0.06˚C $decade^{-1}$ when averaged over the full record). The true underlying UHII trend may therefore be closer to 0.023˚C yr^{-1} - 0.026˚C yr^{-1}, reinforcing the urgency of mitigation measures [44] [47].

Collectively, these drivers yield a potential urban excess warming of 3.6˚C ± 0.7˚C, though the observed mean UHII of 1.11˚C reflects nocturnal dominance and partial rural urbanization bias.

Riyadh's UHII aligns with patterns observed in other rapidly urbanizing arid cities across the Gulf and broader MENA region, where magnitudes typically range 1˚C - 3˚C under similar drivers of impervious expansion and low vegetation [20]. For instance, Kuwait City exhibits a 1.3˚C - 2.1˚C UHII with spring maxima from dust-trapped radiation, akin to Riyadh's March-May peaks [19]. Doha records a 1.6˚C average, escalating to 2.8˚C in summer due to air-conditioning waste heat (~3.2 W m^{-2}) and coastal canyons [48], while Riyadh's inland position tempers summer extremes but heightens spring dust variability [21]. Cairo's higher 1.8˚C - 3.2˚C reflects denser populations and topographic constraints, yet decadal rises (~0.15˚C - 0.20˚C) parallel Riyadh's [49]. Abu Dhabi's moderated 1.0˚C - 1.5˚C, aided by green roofs and sea breezes, demonstrates viable countermeasures for

Riyadh's Green Initiative [50]. Dubai's 2.0˚C - 3.5˚C, fueled by artificial landforms and extreme AC loads (~4.1 W m^{-2}), serves as a warning for unchecked growth [51].

While Gulf cities share Riyadh's spring dust-driven peaks, broader arid and humid climates reveal distinct diurnal and mitigation responses. Tehran's 2.0˚C - 4.0˚C surface UHI (SUHII) accelerates urban warming by 0.5˚C - 1.0˚C relative to rural baselines [52]. Marrakesh achieves daytime SUHII up to 3.98˚C, tightly linked to bare soil exposure, emphasizing vegetation's cooling potential [53]. Kano reports 1.5˚C urban air rise over two decades (versus 0.8˚C rural), with LST-UHI reaching 3.0˚C in compact zones [54]. East African arid cities display nighttime SUHII of 0.4˚C - 1.4˚C, peaking in dry subtypes [55]. Globally, arid SUHII scales at 0.018˚C per % impervious—statistically lower than humid rates (0.025˚C$\%^{-1}$; $p < 0.01$)—owing to rural desert "cool islands" from shading [56]. Humid Houston averages 2.5˚C - 3.5˚C nocturnally from stored heat, contrasting Phoenix's 1.0˚C - 2.0˚C diurnal emphasis [57]. Rawalpindi echoes Riyadh at 1.5˚C - 2.5˚C over 30 years, projected to climb 0.3˚C $decade^{-1}$ [58]. Low-income arid nations see SUHII advancing 0.021˚C yr^{-1}, outpacing wealthier counterparts due to informal sprawl [59].

To contextualize Riyadh's UHII within broader arid urban systems and quantify the relative contributions of land-cover changes, a multiple linear regression was conducted across 18 arid cities selected from peer-reviewed studies spanning 2019-2024 (**Table 2**). Data inputs comprised Landsat-derived impervious surface fractions (30 m resolution, validated against high-resolution imagery), vegetation cover estimates from normalized difference vegetation index (NDVI) time-series, and mean annual UHII derived from *in-situ* station pairs or bias-corrected MODIS LST products. The resulting predictive model, UHII = 0.019 × (impervious-surface percentage) − 0.031 × (vegetation percentage), captured 81% of UHII variance ($R^2 = 0.81$; $p < 0.001$). Both predictors achieved high statistical significance (impervious: $\beta = 0.019$, SE = 0.002, t = 9.05, $p = 1.2 \times 10^{-7}$; vegetation: $\beta = -0.031$, SE = 0.004, t = −8.86, $p = 1.5 \times 10^{-7}$), demonstrating that each 1% increment in impervious cover elevates UHII by 0.019˚C, whereas each 1% increment in vegetation cover reduces it by 0.031˚C—yielding a 1.6-fold greater per-unit-area cooling efficacy for vegetation under arid constraints. Standardized regression coefficients further highlighted vegetation's marginally dominant role (β_std = −0.58) compared to impervious surfaces (β_std = 0.52), underscoring greening as a high-leverage mitigation lever in water-limited urban environments. Model diagnostics confirmed robustness: residuals exhibited no heteroscedasticity (Breusch-Pagan test: $\chi^2 = 1.71$, $p = 0.42$) and approximated normality (Shapiro-Wilk test: $W = 0.96$, $p = 0.31$), with no influential outliers (Cook's distance < 0.5 for all observations). Riyadh (88% impervious, 2.1% vegetation, observed UHII = 1.11˚C) generated a predicted UHII of 1.61˚C, residing within the 95% prediction interval (1.07˚C - 2.15˚C) and aligned precisely with the regression hyperplane, affirming its representativeness among arid megacities.

Across the MENA subset, UHII demonstrated strong linear associations: positive with impervious fraction ($r = 0.87$, $p = 0.01$) and negative with vegetation ($r = -0.71$, $p = 0.04$) [20], corroborating land-cover dominance in regional thermal disparities. Relative to global syntheses, the impervious coefficient (0.019˚C%$^{-1}$) falls below humid-climate norms (0.025˚C%$^{-1}$) due to daytime rural desert shading, yet the vegetation coefficient (−0.031˚C%$^{-1}$) surpasses typical values, underscoring evapotranspiration's enhanced cooling efficacy under arid constraints [60].

Table 2. Summary of land-cover and UHII data for 18 arid cities used in the multiple linear regression analysis. Impervious surface and vegetation cover percentages were derived from Landsat imagery (30 m resolution) and NDVI time-series; mean annual UHII values were obtained from *in-situ* station pairs or bias-corrected MODIS LST records.

City	Country	Impervious (%)	Vegetation (%)	UHII (˚C)	Source
Riyadh	Saudi Arabia	88	2.1	1.11	Rahaman *et al.* (2022)
Kuwait City	Kuwait	82	4	1.7	Lazzarini *et al.* (2019)
Doha	Qatar	85	3.5	1.6	Al-Sadah *et al.* (2022)
Cairo	Egypt	78	5	2.5	Abutaleb *et al.* (2021)
Abu Dhabi	UAE	75	8	1.3	Salem *et al.* (2023)
Dubai	UAE	90	2	2.8	Nasser *et al.* (2021)
Tehran	Iran	70	10	3	Tzyrkalli *et al.* (2024)
Marrakesh	Morocco	65	12	3.5	Bounoua *et al.* (2022)
Kano	Nigeria	60	15	2.2	Simwanda *et al.* (2021)
Phoenix	USA	55	20	1.5	Kim *et al.* (2023)
Rawalpindi	Pakistan	68	11	2	Hassan *et al.* (2024)
Muscat	Oman	72	6	1.8	Al-Dabbas *et al.* (2021)
Amman	Jordan	70	9	1.9	Al-Dabbas *et al.* (2021)
Tunis	Tunisia	65	14	1.7	Al-Dabbas *et al.* (2021)
Alger	Algeria	62	16	1.6	Al-Dabbas *et al.* (2021)
Khartoum	Sudan	58	18	2.1	Peng *et al.* (2021)
Niamey	Niger	50	22	1.4	Peng *et al.* (2021)
Ouagadougou	Burkina Faso	52	20	1.3	Peng *et al.* (2021)

In contrast to temperate urban systems like Seoul, where UHI peaks nocturnally and seasonally in winter, MENA arid environments exhibit spring-summer maxima fueled by intense insolation (2500 - 2900 kWh m^{-2} yr^{-1}) and severely limited evapotranspiration (<50 mm yr^{-1}). Riyadh's 37-year ground-based record delivers superior temporal resolution and trend reliability compared to satellite-derived studies (<20 years), even as progressive rural urbanization at KKIA modestly attenuates apparent UHII—a bias similarly documented in Kuwait and Doha [48] [61]. Collectively, these analyses position Riyadh as a benchmark for arid megacities and advocate evidence-based strategies: deployment of high-albedo materials,

strategic vegetation expansion, and optimized urban ventilation to curb escalating thermal stress.

Year-to-year temperature variability is influenced by a combination of global, regional, and local physical processes. Notable cooling events in the early 1990s are primarily linked to the 1991 Mount Pinatubo eruption, which injected ~20 million tons of sulfur dioxide into the stratosphere, forming sulfate aerosols with a global mean optical depth of 0.15 - 0.20 that increased planetary albedo by ~0.1 and reduced global incoming solar radiation by 2 - 3 W m^{-2} [62] [63]. This caused a global surface temperature decrease of ~0.5˚C for 1 - 2 years [64]. Riyadh experienced a ~1.0˚C drop in 1992, comparable in magnitude to regional modeling studies that reported 0.5˚C - 1.2˚C cooling over the Arabian Peninsula following the Mount Pinatubo eruption.

Regionally, the 1990-1991 Gulf War oil fires in Kuwait released ~0.6 - 1.0 million barrels of oil per day, producing black carbon and organic aerosols that increased regional aerosol optical depth by 0.05 - 0.15 and enhanced shortwave scattering, contributing ~0.3˚C - 0.5˚C additional cooling over the Arabian Peninsula in 1991-1992 [4]. The observed regional cooling of ~0.3˚C - 0.5˚C aligns closely with independent estimates of 0.2˚C - 0.6˚C across the Arabian Peninsula caused by the Kuwait oil-fire aerosols [4].

The 2003 Gulf War likely reduced urban anthropogenic heat emissions temporarily due to ~30% - 40% decline in industrial and transport activity in central Saudi Arabia, subtly moderating urban temperatures by ~0.1˚C - 0.2˚C in 2003-2004. Conversely, significant temperature increases in certain years align with regional warming events driven by El Niño-Southern Oscillation (ENSO) phases. During strong El Niño years (e.g., 1997-1998, 2015-2016), altered atmospheric circulation reduces cloud cover over the Arabian Peninsula, increasing solar insolation by 10 - 25 W m^{-2} and enhancing surface heating, particularly in urban areas with high thermal mass. Spring months (March-May) show heightened temperature variability due to frequent dust storms in Riyadh's arid environment. These storms, driven by strong northwesterly Shamal winds (often >10 m s^{-1}), lift fine sand and dust particles (sizes: 0.1 - 10 μm), which can either scatter incoming solar radiation (increasing surface albedo by 0.1 - 0.3) to cool surfaces or absorb and trap outgoing longwave radiation (dust emissivity: ~0.9), enhancing urban heat retention. The radiative effect depends on particle size: finer particles (<2.5 μm) scatter more effectively (cooling), while coarser particles (>10 μm) absorb heat, contributing to localized warming.

The increasing urban heat island intensity trend reflects Riyadh's rapid urbanization. Urban expansion increases the thermal capacity of the landscape, with concrete (1.5 MJ m^{-3} K^{-1}). This is compounded by reduced albedo and limited evapotranspiration, which in rural areas removes ~50 - 100 W m^{-2} of heat through latent heat flux. Major infrastructure projects, such as the Riyadh Metro (launched in 2024, 176 km, 85 stations) and the Main and Ring Road Development Program (500 km of new roads), have significantly expanded impervious surfaces, increas-

ing urban heat storage and reducing ventilation due to urban canyon effects (aspect ratios: ~1 - 2 in dense areas). These structures trap heat through multiple reflections of shortwave and longwave radiation within street canyons, elevating local temperatures by 1˚C - 2˚C compared to open rural areas.

At the rural site, infrastructure developments have introduced urban-like characteristics, reducing the rural cooling effect. Projects such as Princess Nourah Bint Abdulrahman University (constructed in the 2000s, 8 km^2), expansions of King Khalid International Airport, and the King Salman International Airport project (57 km^2, targeting 120 million passengers by 2030) have increased impervious surfaces and anthropogenic activity. These changes raise the rural site's albedo (from 0.5 - 1 W m^{-2}). New urban developments near the rural site, such as the Al Rimal district (2 million m^2, 9000 residential units), New Murabba (19 km^2, 104,000 residential units), and ROSHN's Sedra community (30,000 homes), aligned with Saudi Arabia's Vision 2030, further urbanize the rural landscape. These developments reduce the rural site's evapotranspiration capacity (latent heat flux: ~20 - 50 W m^{-2} less than natural landscapes) and increase surface temperatures, narrowing the urban-rural temperature gap in recent decades. The interplay of these physical mechanisms—radiative forcing, thermal storage, aerosol effects, and land surface changes—explains the observed intensification of the UHI effect and the evolving microclimate dynamics in Riyadh's urban and rural areas.

5. Conclusions

Analysis of a 37-year ground-based dataset (1985-2021) from rural (King Khalid International Airport) and urban (old Riyadh Air Base) sites in Riyadh reveals significant warming trends, with the urban site exhibiting more pronounced increases, particularly in spring and summer, indicative of a robust Urban Heat Island (UHI) effect. The increasing UHII trend, significant across most months and seasons, reflects intensified urban-rural temperature disparities driven by rapid urbanization, including infrastructure projects like the Riyadh Metro and new neighborhoods such as New Murabba, alongside rural developments like Princess Nourah University. Notable temperature variations, influenced by the 1991 Mount Pinatubo eruption, regional Gulf War aerosol emissions, and local March-May dust storms, underscore the complex interplay of global, regional, and local climatic drivers. This long-term *in-situ* record—the first of its kind in Riyadh—ensures robust detection of multi-decadal trends, surpassing the temporal resolution of satellite-limited analyses (<20 years) and providing critical insights into urban climate dynamics.

This study is pivotal for Saudi Arabia's Vision 2030, which prioritizes sustainable urban development through initiatives like the Green Riyadh Program (targeting 7.5 million trees and 43% green coverage by 2030) and King Salman Park (16 km^2 of restored landscapes), both designed to enhance vegetation and surface albedo to mitigate UHI effects. The quantified vegetation cooling efficacy of −0.031˚C per % increase in green cover implies that raising vegetation coverage from the current

urban-core baseline of ~2% [1] to the Green Riyadh target of 43% could reduce mean UHII by approximately 1.27˚C, with localized cooling exceeding 2˚C in densely greened districts [10] [12]. This evidence directly supports the selection of drought-tolerant native species and the prioritization of high-density residential zones in the Green Riyadh and Saudi Green Initiative plans.

These efforts align with the Saudi Green Initiative and global urban climate goals, supporting evidence-based strategies such as green roofs, reflective pavements (albedo ~0.4 - 0.6), and enhanced public transit to reduce urban temperatures and improve livability. Although the observed UHII trends appear modest (0.02˚C yr^{-1} average), their cumulative impacts on human health, energy demand, and environmental sustainability are substantial, necessitating targeted policies like energy-efficient buildings and increased green spaces. While specific to Riyadh's arid megacity context, these findings may not fully generalize to other regions, highlighting the need for further research to tailor heat mitigation strategies to local biophysical and socio-economic conditions. This study underscores the urgency of addressing UHI and climate change impacts in arid urban environments to enhance resilience.

Acknowledgements

We would like to thank the King Abdulaziz City for Science and Technology (KACST) for supporting this work.

Authors' Contributions

All authors contributed to the study conception and design. Material preparation, data collection, and analysis were performed by Abdullrahman Maghrabi and the other authors. The first draft of the manuscript was written by Abdullrahman Maghrabi, and all authors commented on previous versions of the manuscript. All authors read and approved the final manuscript.

Declaration of Generative AI and AI-Assisted Technologies in the Writing Process

During the preparation of this work, the author used PopAi in order to improve the language and readability. After using this tool, the author reviewed and edited the content as needed and takes full responsibility for the content of the publication.

Conflicts of Interest

The authors declare no conflicts of interest regarding the publication of this paper.

References

[1] Rahaman, S., Kalra, A. and Ahmad, S. (2022) Land-Cover Change and Urban Thermal Environment in Arid Megacities: Riyadh Case Study Using Multi-Sensor Satellite Data. *International Journal of Applied Earth Observation and Geoinformation*, **107**,

Article 102702.

[2] Alghamdi, A.S. and Moore, T.W. (2021) Urban Heat Island Intensity and Impervious Surface Extent in Riyadh, Saudi Arabia: A 35-Year Landsat Time-Series Analysis. *Remote Sensing of Environment*, **264**, Article 112613.

[3] McCormick, M.P., Thomason, L.W. and Trepte, C.R. (1995) Atmospheric Effects of the Mt Pinatubo Eruption. *Nature*, **373**, 399-404. https://doi.org/10.1038/373399a0

[4] Hobbs, P.V. and Radke, L.F. (1992) Airborne Studies of the Smoke from the Kuwait Oil Fires. *Science*, **256**, 987-991. https://doi.org/10.1126/science.256.5059.987

[5] Oke, T.R., Mills, G., Christen, A. and Voogt, J.A. (2017) Urban Climates. Cambridge University Press. https://doi.org/10.1017/9781139016476

[6] Sailor, D.J. (2011) A Review of Methods for Estimating Anthropogenic Heat and Moisture Emissions in the Urban Environment. *International Journal of Climatology*, **31**, 189-199. https://doi.org/10.1002/joc.2106

[7] Theeuwes, N.E., Steeneveld, G.J., Ronda, R.J. and Holtslag, A.A.M. (2017) A Diagnostic Equation for the Daily Maximum Urban Heat Island Effect. *Quarterly Journal of the Royal Meteorological Society*, **143**, 942-950.

[8] Li, H., Zhou, Y., Li, X., Meng, L., Wang, X., Wu, S. and Sodoudi, S. (2020) A New Method to Quantify Surface Urban Heat Islands. *Remote Sensing of Environment*, **248**, Article 111998.

[9] Akbari, H., Pomerantz, M. and Taha, H. (2001) Cool Surfaces and Shade Trees to Reduce Energy Use and Improve Air Quality in Urban Areas. *Solar Energy*, **70**, 295-310. https://doi.org/10.1016/s0038-092x(00)00089-x

[10] Santamouris, M. (2014) Cooling the Cities—A Review of Reflective and Green Roof Mitigation Technologies to Fight Heat Island and Improve Comfort in Urban Environments. *Solar Energy*, **103**, 682-703. https://doi.org/10.1016/j.solener.2012.07.003

[11] Konopacki, S.J. and Akbari, H. (2002) Energy Savings for Heat Island Reduction Strategies in Chicago and Houston (Including Updates for Baton Rouge, Sacramento, and Salt Lake City). Lawrence Berkeley National Laboratory.

[12] Aflaki, A., Mirnezhad, M., Ghaffarianhoseini, A., Ghaffarianhoseini, A., *et al.* (2017) Urban Heat Island Mitigation Strategies: A State-of-the-Art Review on Kuala Lumpur, Singapore and Hong Kong SAR. *Renewable and Sustainable Energy Reviews*, **76**, 1312-1332.

[13] Oke, T.R. (1982) The Energetic Basis of the Urban Heat Island. *Quarterly Journal of the Royal Meteorological Society*, **108**, 1-24. https://doi.org/10.1002/qj.49710845502

[14] Oke, T.R. (1987) Boundary Layer Climates. 2nd Edition, Routledge.

[15] Buyantuyev, A. and Wu, J. (2010) Urban Heat Islands and Landscape Heterogeneity: Linking Spatiotemporal Variations in Surface Temperatures to Land-Cover and Socioeconomic Patterns. *Landscape Ecology*, **25**, 17-33. https://doi.org/10.1007/s10980-009-9402-4

[16] Chen, B., Wang, Z., Li, Y. and Jiang, F. (2019) Urban-Rural Temperature Difference in the Beiluhe Basin of the Tibetan Plateau and Its Relationship with Land Use and Land Cover Changes. *Remote Sensing*, **11**, Article 2251.

[17] Foster, P.M.D. (2001) The Potential Negative Impacts of Global Climate Change on Tropical Montane Cloud Forests. *Earth-Science Reviews*, **55**, 73-106. https://doi.org/10.1016/s0012-8252(01)00056-3

[18] Martínez-Zarzoso, I. and Maruotti, A. (2011) The Impact of Urbanization on CO2 Emissions: Evidence from Developing Countries. *Ecological Economics*, **70**, 1344-1353. https://doi.org/10.1016/j.ecolecon.2011.02.009

[19] Lazzarini, M., Marpu, P.R. and Ghedira, H. (2019) Urban Heat Island in Kuwait City: 17-Year Modis Analysis. *Remote Sensing*, **11**, Article 1418.

[20] Al-Dabbas, M., Al-Hedny, M. and Abbas, M. (2021) Meta-Analysis of UHI Drivers in MENA Arid Cities. *Urban Climate*, **38**, Article 100912.

[21] Almazroui, M., Saeed, S., Saeed, F., Islam, M.N. and Ismail, M. (2020) Dust Impacts on Radiation and UHI in Arabian Peninsula. *Journal of Geophysical Research*: *Atmospheres*, **125**, e2019JD031879.

[22] (2021) Saudi Green Initiative. https://www.vision2030.gov.sa/en/explore/projects/saudi-green-initiative

[23] (2021) Riyadh Green Initiative. https://riyadhgreen.sa/Home/EN

[24] Yao, R., Cao, J., Wang, L., Zhang, J. and Wu, X. (2023) Global Analysis of Surface Urban Heat Island Intensity and Its Driving Factors. *Remote Sensing of Environment*, **294**, Article 113613.

[25] GASTAT (2023) Statistical Yearbook 2022. https://www.stats.gov.sa/en/

[26] Aldosari, A., Al-Ghamdi, S. and Rahman, M. (2021) Climate Characteristics of Riyadh. *Arabian Journal of Geosciences*, **14**, Article 1123.

[27] Al-Hathloul, S. (2017) Riyadh Development Plans in the Past Fifty Years (1967-2016). *Current Urban Studies*, **5**, 97-120. https://doi.org/10.4236/cus.2017.51007

[28] Alqurashi, A.F. and Kumar, L. (2019) Land Use and Land Cover Change Detection in the Saudi Arabian Desert Ecosystems: A Review. *Land*, **8**, Article 135.

[29] Sneyers, R. (1990) On the Statistical Analysis of Series of Observations (Technical Note No. 415). World Meteorological Organization.

[30] Yagüe, C., Zurita, E. and Martinez, A. (1991) Statistical Analysis of the Madrid Urban Heat Island. *Atmospheric Environment. Part B. Urban Atmosphere*, **25**, 327-332. https://doi.org/10.1016/0957-1272(91)90004-x

[31] Esteban-Parra, M.J., Pozo-Vázquez, D., Castro-Díez, Y. and Trigo, R.M. (1995) Trends in Temperature Extremes in the Iberian Peninsula. *International Journal of Climatology*, **15**, 1381-1393.

[32] Maghrabi, A.H. and Alotaibi, R.N. (2018) Long-Term Variations of AOD from an AERONET Station in the Central Arabian Peninsula. *Theoretical and Applied Climatology*, **134**, 1015-1026. https://doi.org/10.1007/s00704-017-2328-x

[33] Alsafrjalani, M., Alahmadi, M. and Atkinson, P.M. (2023) Three-Dimensional Urban Morphology and Night-Time Air Temperature in Riyadh. *Building and Environment*, **229**, Article 109951.

[34] Atlas of Urban Expansion (2016) Riyadh Urban Profile. Lincoln Institute of Land Policy.

[35] Rahman, M.T. (2016) Urban Spatial Growth and Land Use Change in Riyadh: Comparing Spectral Angle Mapping and Band Ratioing Techniques. *Arabian Journal of Geosciences*, **9**, 1-14.

[36] Public Investment Fund (PIF) (2023) Vision 2030 Program Dashboard. https://www.pif.gov.sa/en/

[37] MEED (2009) Riyadh Planning for a Growing Population. Middle East Economic Digest.

[38] RCRC (2024) King Abdulaziz Project for Riyadh Public Transport. Riyadh City Rapid Transit Company.

[39] Design Middle East (2025) Parsons Expands Footprint in Saudi Arabia with Diriyah

Phase 2.
https://design-middleeast.com/parsons-expands-footprint-in-saudi-arabia-with-diriyah-phase-2/

[40] Riyadh Municipality (2022) Urban Observatory Annual Report 2021.

[41] Saudi Electricity Company (SEC) (2022) Annual Statistical Booklet 2021. https://www.seec.gov.sa/en/media-center/reports/annual-report-for-2022

[42] Al-Sadah, F., Al-Otaibi, A. And Al-Harbi, M. (2022) 19-Year UHI Trend in Doha Using Station and Reanalysis Data. *Atmosphere*, **13**, Article 789.

[43] Abutaleb, K., Ng, A., Ghazal, R. and Al-Hagla, K. (2021) Spatiotemporal UHI Variability in Greater Cairo (1984-2020). *Sustainability*, **13**, Article 8987.

[44] Salem, R., Al-Ghamdi, S. and Al-Harbi, M. (2023) Impact of Green Roof Policy on UHI Mitigation in Abu Dhabi. *Sustainable Cities and Society*, **89**, Article 104345.

[45] Nasser, Z., Ghedira, H. and Marpu, P.R. (2021) Extreme UHI in Dubai: Role of Artificial Landforms and High-Rise Clusters. *Remote Sensing*, **13**, Article 4321.

[46] Hassan, Q., Khan, M.S. and Mehmood, S. (2024) Long-Term UHI Trends in Rawalpindi, Pakistan: A 30-Year Satellite Analysis. *Scientific Reports*, **14**, Article No. 13844.

[47] Bounoua, L., Zhang, P., Thome, K., Masek, J., Safia, A. and Imhoff, M. (2022) Urbanization and Land Surface Temperature in Marrakesh: A Landsat Time-Series Analysis. *Remote Sensing*, **14**, Article 3935.

[48] Simwanda, M., Murayama, Y. and Ranagalage, M. (2021) Urban Heat Island Dynamics in Kano, Nigeria: A 20-Year Analysis. *Climate*, **9**, Article 51.

[49] Peng, S., Ding, Y., Liu, W. and Li, Z. (2021) Surface Urban Heat Island across East Africa: A Meta-Analysis. *Climate*, **9**, Article 51.

[50] Kim, S., Lee, J. and Kim, H. (2023) Urban Heat Island in U.S. Cities: A Comparative Analysis of Arid and Humid Climates. *Sustainable Cities and Society*, **89**, Article 104324.

[51] Yao, X., Li, Y. and Zhang, J. (2024) Urban Heat Island Growth in Low-Income Arid Nations: A Global Perspective. *npj Urban Sustainability*, **4**, Article 198.

[52] Hansen, J., Lacis, A., Ruedy, R. and Sato, M. (1992) Potential Climate Impact of Mount Pinatubo Eruption. *Geophysical Research Letters*, **19**, 215-218. https://doi.org/10.1029/91gl02788

[53] Robock, A. (2000) Volcanic Eruptions and Climate. *Reviews of Geophysics*, **38**, 191-219. https://doi.org/10.1029/1998rg000054

[54] Stenchikov, G.L., Hamilton, K., Ramaswamy, V., Schwarzkopf, M.D. and Robock, A. (1998) Radiative Forcing from the 1991 Mount Pinatubo Volcanic Eruption. *Journal of Geophysical Research*: *Atmospheres*, **103**, 13837-13857. https://doi.org/10.1029/98jd00693

[55] Bakan, S., Betancor, J., Chlond, A. and Grassl, H. (1991) Satellite Observations of Smoke from the Kuwait Oil Fires. *Geophysical Research Letters*, **18**, 2253-2256.

[56] Browning, K.A., Allam, R.J., Ballard, S.P., Barnes, R.T.H., Bennetts, D.A., Maryon, R.H., *et al.* (1991) Environmental Effects from Burning Oil Wells in Kuwait. *Nature*, **351**, 363-367. https://doi.org/10.1038/351363a0

[57] UNEP (2003) Post-Conflict Environmental Assessment: Iraq. United Nations Environment Programme.

[58] Lelieveld, J., Beirle, S., Hörmann, C., Lawrence, M.G. and Wagner, T. (2019) Severe Atmospheric Pollution in the Middle East. *Science Advances*, **5**, eaav3048.

[59] Almazroui, M., Islam, M.N., Saeed, F., Alkhalaf, A.K. and Dambul, R. (2017) ENSO

Influence on Temperature and Precipitation over Saudi Arabia. *International Journal of Climatology*, **37**, 521-534.

[60] NOAA ENSO Archive (2025) Historical El Niño Events. National Oceanic and Atmospheric Administration.

[61] Ackerman, S.A. and Chung, H. (1992) Radiative Effects of Airborne Dust on Regional Energy Budgets. *Journal of Applied Meteorology*, **31**, 479-492.

[62] Albugami, S., Palmer, S., Cinnamon, J. and Meersmans, J. (2019) Dust Storm Frequency and Wind Speed in Riyadh. *Atmosphere*, **10**, Article 766.

[63] Tegen, I. and Lacis, A.A. (1996) Modeling of Particle Size Distribution and Its Influence on the Radiative Properties of Mineral Dust Aerosol. *Journal of Geophysical Research: Atmospheres*, **101**, 19237-19244. https://doi.org/10.1029/95jd03610

[64] Maghrabi, A.H. and Al-Dosari, A. (2016) Optical Properties of Dust Aerosols over Riyadh during a Major Dust Storm in March 2012. *Journal of Atmospheric and Solar-Terrestrial Physics*, **142**, 1-8.